PHOTOSYNTHETICA
International Journal for Photosynthesis Research

DOI 10.32615/ps.2026.020 PHOTOSYNTHETICA 64 (SI): 113-125, 2026

Special issue in honor of Prof. Suleyman I. Allakhverdiev

Differentiating seasonal trends and environmental responses in wheat through longitudinal chlorophyll *a* fluorescence phenotyping

M. ZIVCAK[*,+], M. KOVAR[*], A. DAS[*], M. BARBORICOVA[*], D. PALOVOVA[*], P. HAUPTVOGEL[**], and M. BRESTIC[*]

Institute of Plant and Environmental Sciences, Slovak University of Agriculture in Nitra, A. Hlinku 2, 94976 Nitra, Slovakia[*]
Research Institute of Plant Production, National Agricultural and Food Centre, Bratislavská cesta 122, 92168 Piestany, Slovakia[**]

Abstract

Broad adoption of chlorophyll fluorescence kinetics in crop phenotyping remains limited by inconsistent parameter definitions and insufficient physiological validation. This study employed a longitudinal phenomic approach to evaluate the diagnostic value of rapid chlorophyll *a* fluorescence kinetics across diverse wheat genotypes throughout a spring growing season. By combining JIP-test parameters with detailed growth analysis, we built a statistical framework quantifying the predictive power and unexplained variance of biophysical parameters derived from the JIP-test, with an emphasis on performance-estimating indices. Results show that conventional parameters, such as maximum quantum yield of primary photochemistry, remain stable during vegetative growth and are highly sensitive to terminal senescence, yet display considerable noise under transient environmental fluctuations. Conversely, integrative indicators, particularly the total performance index, revealed clear seasonal trends and strong correlations with growth dynamics. By grouping JIP-test parameters functionally, this study offers a rational framework for selecting biophysical indices suited to specific breeding or research goals.

Keywords: chlorophyll *a* fluorescence; high-throughput phenotyping; JIP-test; photosynthetic performance; total performance index; wheat.

Introduction

High-throughput phenotyping is essential for modern crop breeding programs aimed at improving wheat photosynthetic performance. One of the most promising techniques is the analysis of fast chlorophyll *a* fluorescence kinetics, which acts as a "biophysical signature" of the plant's potential to convert light into chemical energy (Stirbet and Govindjee 2011, Kalaji *et al*. 2016). The high information resolution of the OJIP transient

Highlights

- Longitudinal phenotyping distinguished seasonal trends from transient environmental noise
- Total performance index showed a strong seasonal trend, correlating with growth patterns
- Some fluorescence parameters can track even moderate environmental fluctuations

Received 6 April 2026
Accepted 21 July 2026
Published online 8 September 2026

[+]Corresponding author
e-mail: marek.zivcak@uniag.sk

Abbreviations: ABS – absorption; *ANOVA* – analysis of variance; CS – cross-section; DAS – days after sowing; *df* – driving force of photosynthesis; ETo – electron transport flux; F_m – maximum fluorescence; F_o – initial fluorescence; F_v – variable fluorescence; JIP-test – mathematical analysis of the OJIP fluorescence transient; OJIP – fast chlorophyll *a* fluorescence induction kinetics; PI – performance index; PQ – plastoquinone; RC – reaction centre; SE – standard error of the mean.

Acknowledgements: We thank the Research Institute of Plant Production in Piestany for conducting the field experiments. We also thank our former colleagues Elena Hunkova and Jana Pivkova for their contributions to measurements, sample collection, and processing. This research was supported by the research projects APVV-22-0392 and VEGA 1-0639-26.
Conflict of interest: The authors declare that they have no conflict of interest.

allows the detection of subtle functional alterations through multi-parametric performance indices long before visible symptoms of stress or ageing appear (Strasser *et al.* 1995). Analysed *via* the JIP-test, these kinetic patterns describe the seamless movement and transformation of energy through internal systems, quantifying a plant's overall efficiency and its capacity to manage resource influx (Strasser *et al.* 2004, Tsimilli-Michael 2020). From a structural and functional standpoint, the JIP-test allows noninvasive monitoring of the stepwise reduction of the linear electron transport chain, from the initial capture of light to its transfer through various intermediate carriers and delivery to the final acceptors of PSI (Strasser and Strasser 1995, Schansker *et al.* 2005).

It is clear that a very short timescale (1 second) of measurements limits its direct predictive value for CO_2 assimilation, growth, and yield (Stirbet *et al.* 2018). On the other hand, almost all attempts to identify proxies for photosynthetic productivity, for example, in remote and proximal sensing, are based on parameters with indirect optical indicators (Siebers *et al.* 2021). As with other techniques, there is sufficient evidence that fast fluorescence kinetics analysis can identify declines in photosynthetic capacity due to multiple stress factors (Kalaji *et al.* 2016) or ontogenetic shifts (Koller *et al.* 2020). However, the widespread implementation of the JIP-test is currently hindered by inconsistent parameter definitions and a lack of rigorous physiological validation, a deficiency that frequently leads to interpretative confusion and technical artefacts (Kalaji *et al.* 2014, Tsimilli-Michael 2020).

To assess the functional status and vitality of the physiological apparatus, parameters with a clear link to photochemical performance are needed. Based on the biophysical background and physiological interpretation, we can distinguish several groups of parameters, from which several groups may serve as performance-estimating parameters. Quantum yields and probabilities represent the fundamental probability that absorbed photons are converted into chemical energy, with the maximum quantum yield of primary photochemistry (F_v/F_m) or related parameters (*e.g.*, F_v/F_o) serving as primary indicators of the integrity of the photosynthetic machinery (Butler and Kitajima 1975, Stirbet and Govindjee 2011). Acceptor pool size indicators derived from the geometry of the fluorescence transient, such as the parameter Area or derived normalised parameters, provide an estimate of the relative capacity of the system's electron carriers to process multiple turnovers (Strasser and Strasser 1995, Stirbet and Govindjee 2011). Reaction centre densities quantify the abundance of functional RCs relative to different structural baselines, particularly per light-harvesting antenna chlorophyll (RC/ABS) and per leaf area cross-section (RC/CSo, RC/CSm) (Strasser *et al.* 2004, Kalaji *et al.* 2016). Electron transport-related parameters describe the rate and efficiency of electron movement through the chain per unit area (ETo/CSo, ETo/CSm) or per reaction centres (ETo/RC) (Ceppi *et al.* 2012, Tsimilli-Michael 2020). Performance indices act as sensitive, holistic vitality markers by integrating multiple biophysical potentials into a single numerical value. Two key metrics are the absorption-based performance index (PI_{abs}) and the total performance index (PI_{tot}). The latter is particularly robust, as it accounts for energy conservation efficiency across the entire electron transport chain, up to the final acceptors of PSI (Strasser *et al.* 2000, Tsimilli-Michael and Strasser 2008).

When measured in crop plants, the parameters derived from OJIP fluorescence analysis may provide various categories of physiological information. Within the genotype-specific patterns, we can usually recognise two main signals: environmental responses and developmental responses. Environmental responses describe the immediate or acclimatory adjustments of the photosynthetic machinery to external stressors, such as temperature and light fluctuations, water supply, or the presence of various stress factors even under moderate conditions (Stirbet and Govindjee 2011, Begović *et al.* 2020). In contrast, developmental responses follow characteristic internal patterns as leaves transition from carbon sinks during maturation to carbon sources, eventually dismantling their apparatus during natural senescence (Thomas and Ougham 2014, Viljevac Vuletić and Španić 2020). For instance, performance indices typically peak during full expansion and decline steadily during leaf ageing, a pattern that mirrors the loss of vitality observed under stress (Prakash *et al.* 2003, Zeng *et al.* 2021). Despite the high sensitivity of these biophysical markers, a significant knowledge gap exists regarding the ability to definitively decouple these two response types in moderate or field conditions (Digrado *et al.* 2017, Koller *et al.* 2020). Distinguishing between ontogenetic signatures and environmentally driven responses remains a significant challenge. This ambiguity persists because moderate environmental stressors and natural leaf ageing often produce nearly identical biophysical fingerprints (Živčák *et al.* 2008, Holland *et al.* 2014, Begović *et al.* 2020). This overlap suggests that without better longitudinal integration of measured phenotypic data, the diagnostic potential of fluorescence recordings may be compromised in real-world agricultural or ecological settings (Kalaji *et al.* 2016, Koller *et al.* 2020). Moreover, most of the results in crop plants come from experiments with single or a small number of genotypes. In turn, the genotype diversity in analyses (multi-genotype design) can reveal niche complementarity, thereby producing more transferable results and broader applicability of findings across environments and genotypic backgrounds (Gaudio *et al.* 2019).

In this context, we analysed the data from rapid chlorophyll fluorescence kinetics measured on 30 wheat genotypes, originally conducted to identify the characteristics and specific responses of individual genotypes during the spring growing season. In the data analyses performed specifically for this study, we treated the entire set of genotypes as a single population in order to obtain the average trend of seasonal parameters, while specific genotype responses were not monitored. This approach allowed us to generate a sufficiently robust dataset, which enabled us to perform phenotypic analyses at the level of high throughput phenotyping systems.

Large-scale trait analyses provide richer, more repeatable measurements that reduce the noise typical of low-throughput methods, while inference frameworks, which use big data, help distinguish true cause-and-effect relationships within these traits. When such data are combined with mechanistic knowledge through sensitive analytical approaches, hidden bias from unmeasured factors can be reduced and residual noise minimised, enabling clearer interpretation (Pandey *et al*. 2021, Yoo *et al.* 2022, Zhang *et al*. 2023).

Therefore, the primary objective of this study was to establish a robust biophysical framework for disentangling the overlapping signals of environmental acclimation and ontogenetic development within the photosynthetic apparatus of winter wheat. By leveraging a longitudinal, phenomic-scale approach across a diverse population of 30 wheat genotypes, we tried to identify which chlorophyll fluorescence parameters serve as stable indicators of seasonal growth dynamics and which function as sensitive sensors of transient environmental perturbations.

Specifically, we aimed to evaluate the predictive power of various "performance-based" JIP-test parameters, ranging from primary quantum yields and specific energy fluxes to integrative performance indices, in relation to morphological growth rates and biomass accumulation throughout a complete vegetative-to-reproductive cycle. A central goal was to quantify the "unexplained variance" of these biophysical markers to determine their reliability as phenotyping tools in complex field environments. Through this analysis, we intended to categorise the OJIP-derived parameters into functional groups based on their sensitivity to internal developmental programming *vs*. external stressors.

Ultimately, the study aimed to validate the efficacy of integrative biophysical parameters and performance indices as a high-resolution "photosynthetic fingerprint" that can reduce measurement noise and provide a clear, mechanistic link between the efficiency of the electron transport chain and overall plant productivity, thereby enhancing the precision of modern crop breeding programs.

Materials and methods

Experimental site and plant material: The field research was conducted during a single growing season at an agricultural research facility of the Research Institute of Plant Production in Piestany, Slovakia. The soil at the site was characterised as a fertile silt loam. Field pea (*Pisum sativum* L.) served as the preceding crop to establish a baseline of soil fertility. Following a detailed soil nutrient analysis in the autumn, supplemental fertilisers were applied to ensure nonlimiting conditions for wheat development. Sowing was performed manually on 10 October at a standardised seeding depth and density. The crop successfully emerged in mid-November and underwent a typical overwintering phase. In March, during the tillering stage, nitrogen was applied using ammonium nitrate. To prevent weed competition, the plots were treated in early April with an herbicide tank mix. The experiment reached physiological maturity in July, with the final harvest on 17 July. Weather conditions during the measuring period, as well as the frequency of the measurements (S1–S9) and plant samplings (S1–S8), are shown in Fig. 1.

The study evaluated 30 wheat (*Triticum aestivum* L.) genotypes spanning six ecological groups: Central Europe (Komfort, Biscay, GK Forras, Tamaro), Slovakia (Astella, Malvina, Venistar, Torysa, Vanda, Kosutska, Viglasska cervenoklasa, Samorinska, Vrakunska, Radosinska norma), Northern/Eastern Europe and Central Asia (Griffen, Gedania, Mewa, Echo, Steklovidnaja 24), Southern Europe and the Middle East (Verna, Mottin, Bbyo 17, Dagdas 94, Pehlivan), East Asia (Shaan 8007-7, Chua-bej, Hokushin, Nanbu Komugi), and Mexico (Piopio_4, Shark-4). All genotypes were treated as a single population with equal contributions.

Chlorophyll fluorescence and JIP-test analysis: To evaluate the efficiency of the photosynthetic apparatus, fast chlorophyll *a* fluorescence kinetics were measured using a portable *Handy Pea* fluorimeter manufactured by *Hansatech Instruments* (UK). Measurements were taken on the uppermost fully expanded leaves directly in the field, between 10:00 and 14:00 h. Environmental conditions during measurements fluctuated in terms of both temperature (Fig. 1) and light intensity, ranging from fully sunny days to overcast or partly cloudy conditions. Before the induction of fluorescence, leaves were dark-adapted for 20 min using specialised clips to ensure that all reaction centres were in an open state. Fluorescence was then induced by a one-second pulse of saturating red light at an intensity of 3,500 μmol(photon) m^{-2} s^{-1}.

The resulting induction curves were analysed using the JIP-test protocol (Strasser *et al*. 2000). The primary parameters recorded included the initial fluorescence (F_o) measured at 50 microseconds, the maximum fluorescence

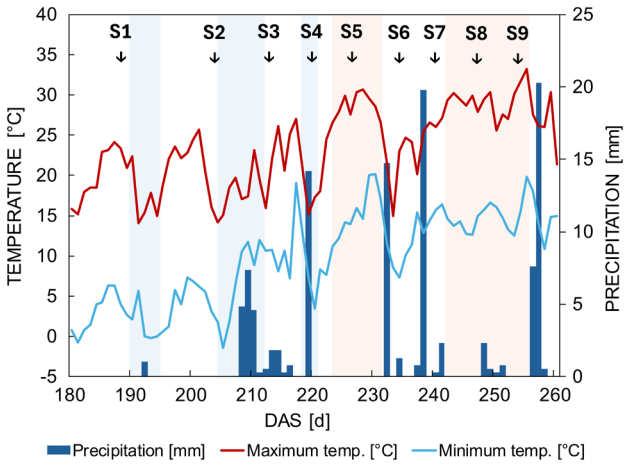

Fig. 1. The records of maximum and minimum temperature (*lines*) and daily precipitation (*columns*) at the site of experiments during the period of measurements and sampling. Fill colour shows deviation from the long-term local average: *blue* for colder periods, *orange* for warmer periods. S1–S9 indicate the dates of field sampling and measurements. Timeline (*x*-axis) spanning early April to mid-June.

(F_m), and the variable fluorescence (F_v), calculated as the difference between F_m and F_o. The functional efficiency was assessed using the F_v/F_m ratio, which represents the maximum photochemical yield of PSII, and the F_v/F_o ratio, which indicates the efficiency of the water-splitting complex. The total area between the fluorescence curve and F_m (Area) was used to estimate the size of the plastoquinone pool. Specific energy fluxes were determined, including the electron transport per active reaction centre (ETo/RC) and the electron transport per cross-section at both initial and maximum levels (ETo/CSo and ETo/CSm). The density of active reaction centres was quantified relative to light absorption (RC/ABS) and leaf cross-sections (RC/CSo and RC/CSm). Furthermore, integrative performance was evaluated using the performance index on an absorption basis (PI_{abs}), the total performance index (PI_{tot}), and the overall driving force of photosynthesis (*df*). Individual parameters were calculated according to the equations summarised by Stirbet and Govindjee (2011). Parameter notation was retained as originally defined by Strasser *et al.* (2004).

Growth analysis and biomass partitioning: A comprehensive growth analysis was performed to track the development of the genotypes throughout their life cycle. Destructive sampling was conducted at regular intervals, with six representative plants collected from each genotype at each sampling event. Leaf area was determined using a linear measurement approach, where the length and maximum width of each leaf blade were recorded and multiplied by a morphometric coefficient to calculate the Area in square meters per plant (Miralles and Slafer 1991). The accuracy of the method was improved by its calibration using image analysis of leaves in part of the plants from each genotype using image analysis software *ImageJ* (National Institutes of Health, Bethesda, MD, USA). To determine biomass accumulation, the plant samples were dried in a forced-air oven at 80°C until a constant mass was reached. These data were then used to calculate the dynamics of leaf area expansion, the total dry matter increment, and the mean daily growth rate.

Statistical analyses: The experiment was arranged in a randomised complete block design with three replications. Each experimental plot measured 2.7 m². A total of 30 genotypes were evaluated, with three plots per genotype. Within each plot, two plants were selected for nondestructive *in situ* measurements, and two additional plants were harvested for destructive growth analysis (totalling six biological replicates per genotype for each method). Consequently, on each sampling date, a total of 180 measurements (30 genotypes × 6 plants) were recorded, and 180 plant samples (30 genotypes × 6 plants) were collected for growth analysis. This sampling procedure was repeated identically across nine sampling dates, spanning from mid-April to mid-June, to capture the temporal dynamics of plant growth and development throughout the study period. The consistent sampling scheme applied at each date ensured comparability of measurements across genotypes and time points, allowing for a robust assessment of genotypic differences in growth-related traits over the course of the growing season.

The experimental data were analysed using analysis of variance (*ANOVA*) to assess the significance of differences between the genotypes and the defined ecological groups. When significant effects were detected at a probability level of P less than 0.05, mean values were compared using the *Duncan* post-hoc test. The correlation analysis was also performed, using correlation indices (r). The deviation from the seasonal trend was calculated using the Theil Inequality Coefficient (U), providing a robust measure of trend data smoothness or noise (Theil *et al.* 1961, Bellocchi *et al.* 2010). All statistical computations and the generation of physiological models were performed using *Statistica 10* (*StatSoft*, USA) and *MS Excel* (*Microsoft*, USA). The results are presented as the arithmetic mean of the replications, along with the standard error (SE) of the mean, to provide a clear indication of the data's precision and variability.

Results

Seasonal dynamics of morphological development and biomass accumulation: The growth trajectory of the winter wheat genotypes during the main growing season followed a highly predictable ontogenetic pattern. Total plant leaf area (Fig. 2*A*) exhibited an initial slow expansion during the overwintering phase, followed by a rapid linear increase after the spring tillering stage (approximately 180 d after sowing, DAS). The leaf area reached its physiological maximum of approximately 0.015 square meters per plant at 215 DAS. Beyond 240 DAS, a sharp decline in leaf area was observed, signifying the onset of canopy-wide senescence during the grain-filling period.

This morphological progression was closely mirrored by the accumulation of cumulative plant dry mass (Fig. 2*B*). Biomass accumulation followed a sigmoidal curve, with a lag phase during winter and an exponential phase in early spring. By the final sampling intervals, cumulative dry mass reached a plateau at approximately 4.75 to 5.0 g per plant. The mean daily plant growth rate (Fig. 2*C*) provided a high-resolution view of vegetative vigour, exhibiting a characteristic bell-shaped distribution. The peak growth rate of 0.11 g per day was achieved between 210 and 230 DAS, several days later compared to the period of maximum leaf area. Interestingly, the temporary temperature variations (Fig. 1) did not cause oscillations in the trajectory of the growing parameters. The subsequent decrease in growth rate after 240 DAS aligns with the transition from vegetative growth to reproductive sink-filling and physiological maturation. The onset of the decrease could be accelerated by the warm period at the end of the vegetative stage (Fig. 1).

Longitudinal analysis of PSII photochemistry and performance indices: To assess the functional integrity of the photosynthetic apparatus throughout the season, we monitored several groups of parameters derived from fast chlorophyll fluorescence kinetics, belonging to different

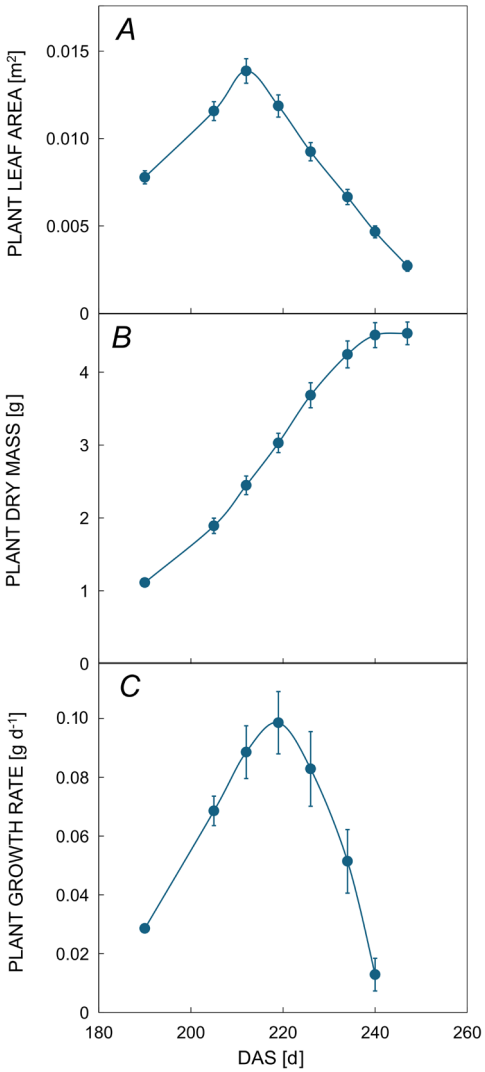

Fig. 2. Seasonal dynamics of plant growth and biomass accumulation in winter wheat. (*A*) Dynamics of total plant leaf area (square meters per plant) illustrating the expansion phase and subsequent senescence. (*B*) Cumulative plant dry mass (g) accumulation over the course of the experiment. (*C*) Mean daily plant growth rate (grams per day) during the period of maximum vegetative vigour. Data points represent the mean values of 30 genotypes, with each genotype represented by 6 sampled plants per interval ($n \approx 180$ per point; 30 genotypes × 6 biological replicates). Error bars indicate the standard error of the mean (SE). DAS – days after sowing.

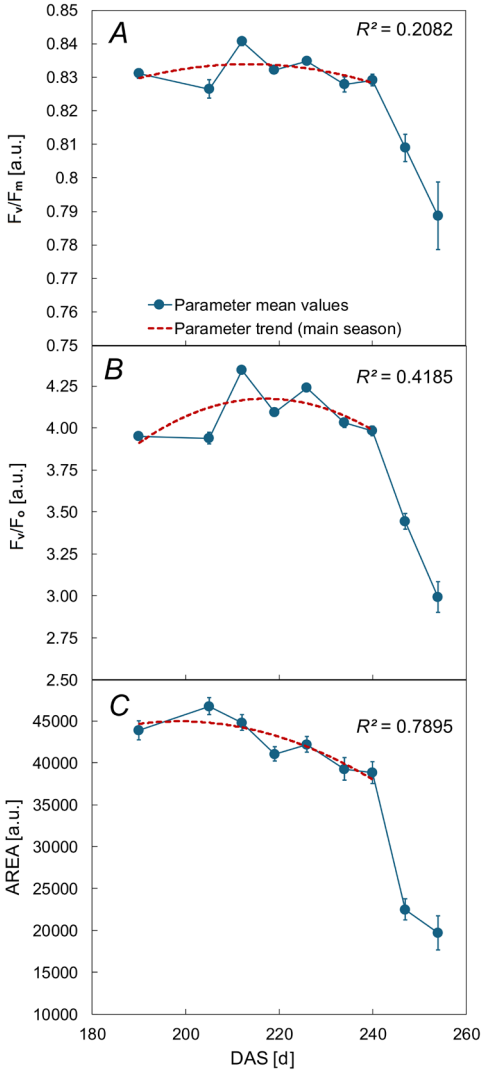

Fig. 3. Seasonal variation in primary photosynthetic efficiency and PSII acceptor pool size. (*A*) Maximum quantum yield of PSII (F_v/F_m), (*B*) ratio of quantum yields of photochemical to nonphotochemical processes (F_v/F_o), and (*C*) the total area above the fluorescence induction curve (Area), representing the size of the plastoquinone (PQ) pool on the reducing side of PSII. *Blue circles* represent the mean value at each time point, calculated across all evaluated genotypes ($n \approx 180$ per point; 30 genotypes × 6 biological replicates), with error bars denoting ± standard error (SE) of the mean. *The dashed red line* shows a third-order polynomial fit (best fit) to the main growing season, excluding the senescence phase, to highlight the overall developmental trend independent of late-season decline. DAS – days after sowing.

groups. The first group comprised basic parameters, including quantum yields and acceptor pool capacity.

The maximum quantum yield of PSII, expressed as F_v/F_m, remained relatively high and stable (averaging 0.82 to 0.83) for the majority of the season (Fig. 3*A*). However, as the crop surpassed 240 DAS, F_v/F_m values dropped significantly to below 0.78, indicating a loss of photochemical efficiency during the late grain-filling stage, likely due to the onset of senescence. A similar, more sensitive trend was observed in the values of the related F_v/F_o parameter (Fig. 3*B*), which showed a steady decline throughout the season. The trend in the total area above the fluorescence induction curve (Area), which represents the size of the plastoquinone (PQ) pool on the reducing side of PSII, followed the seasonal trend, followed by a decline due to leaf senescence (Fig. 3*C*). Some of the unexplained variance (deviation of the measured value from the fitted trend) can be attributed to variability in meteorological conditions (temperature, rainfall), especially the cold/hot

transitions shown in Fig. 1. In addition, the onset of senescence was likely driven by the hot period beginning on day 240.

The second group of indicators assessed were the parameters reflecting electron transport at PSII expressed in different units. The specific electron transport flux per active reaction centre (ETo/RC) remained relatively high during the peak vegetative phase but declined sharply as the crop approached maturity (Fig. 4*A*). More strikingly, the phenomenological electron transport fluxes per leaf cross-section at the initial state (ETo/CSo) and at maximum fluorescence (ETo/CSm) showed exceptionally strong seasonal trends (Fig. 4*B*,*C*). In particular, ETo/CSo exhibited a near-linear decline (R^2 = 0.9541), suggesting a systematic reduction in the electron transport per unit leaf area as the plants aged.

A close view of the period between DAS 185 and 220 (Fig. 4) reveals that ETo/RC acted as a sensitive environmental sensor, with fluctuations mirroring the short-term temperature spikes and dips recorded at the site (Fig. 1). That suggests that the parameter reflects a highly plastic response, adjusting almost instantaneously to the ambient thermal environment. On the other hand, the phenomenological fluxes, especially ETo/CSo, maintained a much smoother, near-linear decline during this same period.

The third group of parameters assessed the trend in the density of active reaction centres (RC) expressed per different units. The density of RCs relative to light absorption (RC/ABS) peaked at approximately 220 DAS before declining (Fig. 5*A*).

Still, this parameter showed high variability across dates, with a strong decrease in the fourth sampling and an increase in the fifth, which deviated from the overall trend. The decrease in RC density due to senescence was clearly evident in the last two samplings. In contrast to the previous, the density of RCs per leaf cross-section (RC/CSo and RC/CSm) followed a decreasing trajectory, maintaining more or less stable values through the mid-vegetative stage, followed by a precipitous drop during the senescence phase (Fig. 5*B*,*C*). The results clearly indicate that RC densities expressed per absorbed light unit (ABS) differ from those expressed per unit area (here denoted as CSo and CSm). Nevertheless, across all three parameters, there is some variance from the predicted seasonal trend, likely due to environmental fluctuations during the season. In this respect, apart from the senescence effects at the end of the season, the number of reaction centres responded more positively to the transition from lower to higher temperatures, as shown by comparing the trends in Fig. 5 with those in Fig. 1.

The last group of parameters assessed was the integrative indicators of plant vitality, denoted as performance indices. The performance index on an absorption basis (PI_{abs}), which integrates reaction centre density and quantum yields, and the closely related total driving force of photosynthesis (*df*), both showed strong seasonal trends (Fig. 6*A*,*B*). Nevertheless, the total performance index (PI_{tot}), which incorporates the efficiency of the terminal electron acceptors of PSI, exhibited the highest seasonal

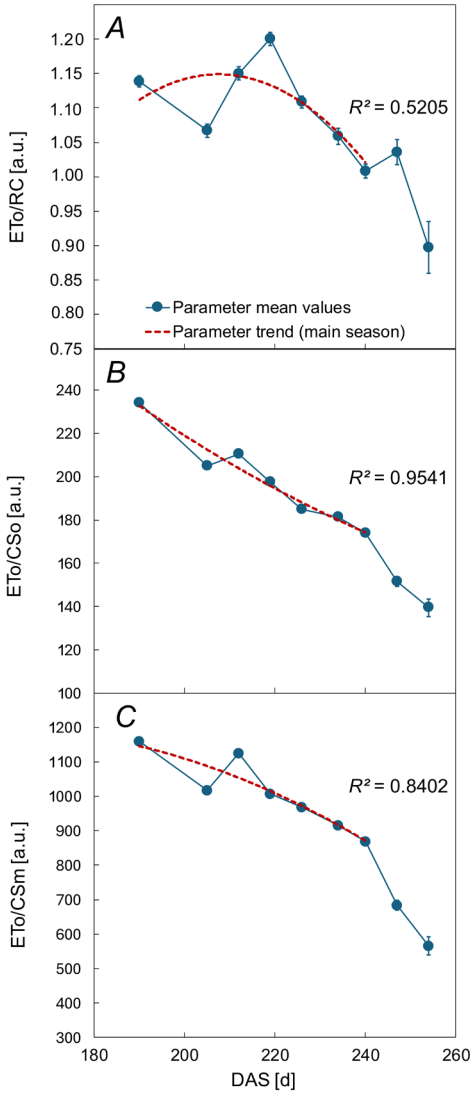

Fig. 4. Dynamics of electron transport fluxes per reaction centre and leaf cross-section. Analysis of energy flux parameters calculated *via* the JIP-test protocol. (*A*) Electron transport flux per active reaction centre (ETo/RC). (*B*) Phenomenological electron transport flux per leaf cross-section at the initial state (ETo/CSo). (*C*) Phenomenological electron transport flux per leaf cross-section at maximum fluorescence (ETo/CSm). Parameters are expressed in arbitrary units (a.u.). *Blue circles* represent the mean value at each time point, calculated across all evaluated genotypes ($n \approx 180$ per point; 30 genotypes × 6 biological replicates), with error bars denoting ± standard error (SE) of the mean. *The dashed red line* shows a third-order polynomial fit (best fit) to the main growing season, excluding the senescence phase, to highlight the overall developmental trend independent of late-season decline. DAS – days after sowing.

predictability (R^2 of 0.95) and remained closely aligned with the crop's physiological age (Fig. 6*C*).

While the temperature variations shown in Fig. 1 had minor effects on the trend in PI_{abs} and *df*, PI_{tot} demonstrated the most robust behaviour; even during the rapid temperature shift observed around DAS 220, the parameter

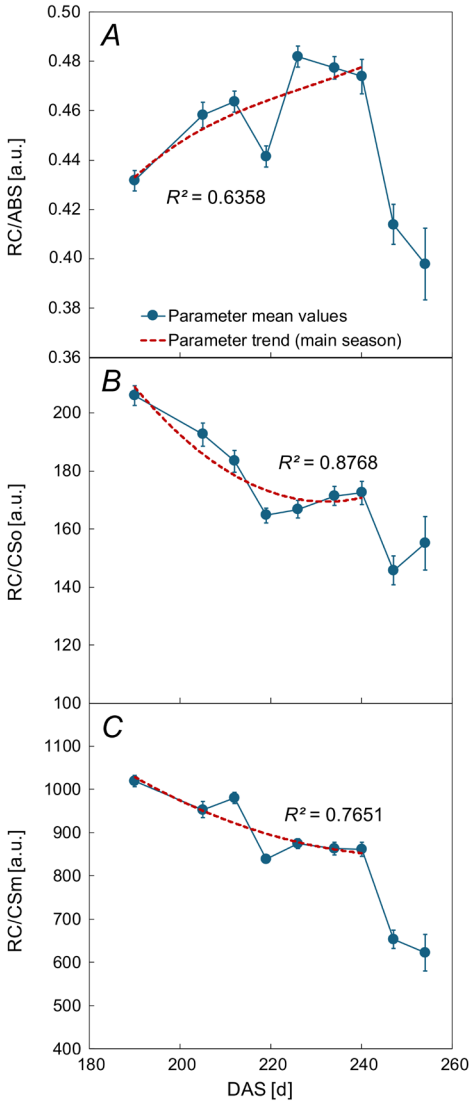

Fig. 5. The density of active reaction centres (RC) relative to light absorption and leaf surface area. (*A*) Density of RCs per chlorophyll unit or absorption (RC/ABS). (*B*) Density of RCs per leaf cross-section at the initial state (RC/CSo). (*C*) Density of RCs per leaf cross-section at maximum fluorescence (RC/CSm). The data illustrate a peak in active RC density during the mid-vegetative stage, followed by a sharp decline during the onset of leaf senescence. *Blue circles* represent the mean value at each time point, calculated across all evaluated genotypes ($n \approx 180$ per point; 30 genotypes × 6 biological replicates), with error bars denoting ± standard error (SE) of the mean. *The dashed red line* shows a third-order polynomial fit (best fit) to the main growing season, excluding the senescence phase, to highlight the overall developmental trend independent of late-season decline. DAS – days after sowing.

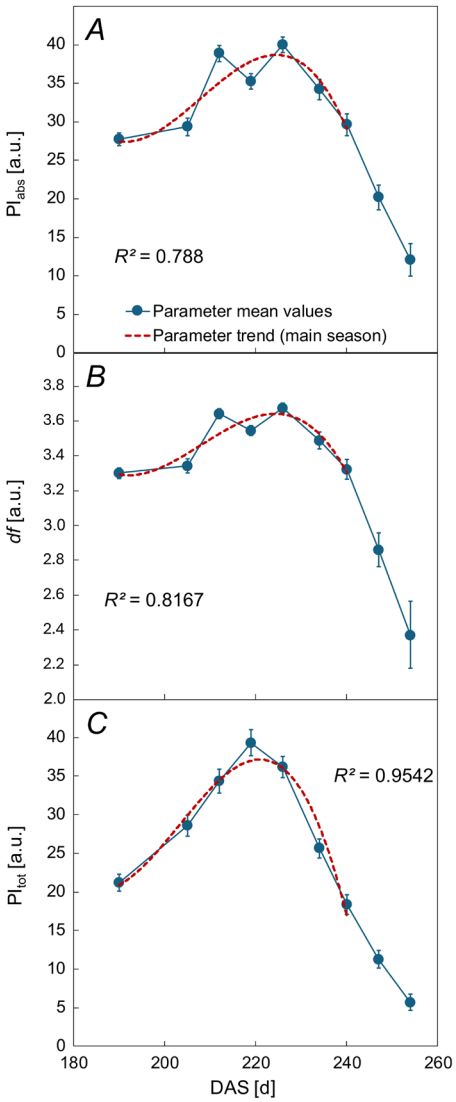

Fig. 6. Integrative photosynthetic performance indices and driving forces calculated from JIP-test transients. (*A*) Performance index on an absorption basis (PI_{abs}), integrating the density of reaction centres, the quantum yield of primary photochemistry, and the probability of electron transport. (*B*) The total driving force of photosynthesis (*df*) based on fluorescence kinetics. (*C*) Total performance index (PI_{tot}), which incorporates the efficiency of the terminal electron acceptors of PSI. *Blue circles* represent the mean value at each time point, calculated across all evaluated genotypes ($n \approx 180$ per point; 30 genotypes × 6 biological replicates), with error bars denoting ± standard error (SE) of the mean. *The dashed red line* shows a third-order polynomial fit (best fit) to the main growing season, excluding the senescence phase, to highlight the overall developmental trend independent of late-season decline. DAS – days after sowing.

continued its smooth trajectory. That suggests that PI_{tot} is capable of disentangling the underlying ontogenetic signal from the transient environmental effects of spring weather fluctuations.

Statistical differentiation of seasonal and environmental sensitivity: The relationships among the biophysical parameters, as well as their correlation with growth rate, were further elucidated using a *Pearson*'s correlation matrix (Fig. 7).

Despite all fluorescence parameters being derived from the same curves, low mutual correlations among most of them indicate that they truly represent independent values quantifying different processes and phenomena of PSII

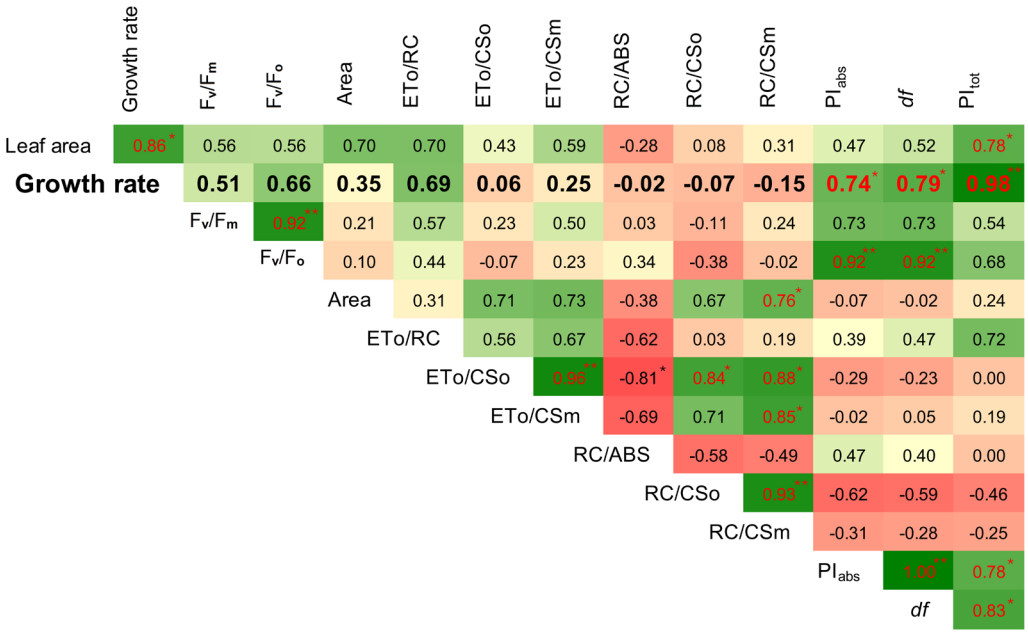

Fig. 7. Correlation matrix between average values of growth parameters and JIP-test fluorescence variables. A heatmap of *Pearson*'s correlation coefficients (*r*) illustrating the relationships between morphological growth traits (Leaf area, Growth rate) and photosynthetic parameters. Colour intensity represents the strength of the correlation, with *green* indicating positive correlations and *red* indicating negative correlations. *The red colour* of the numbers indicates a statistically significant positive relationship between the parameters. Double asterisks (**) indicate $p \leq 0.01$; single asterisks (*) indicate $0.01 < p \leq 0.05$. Correlations were based on average parameter values from seven sampling dates (S1–S7) spanning the main growing season, excluding the senescence phase. F_v/F_m – maximum quantum yield of PSII; F_v/F_o – ratio of quantum yields of photochemical to nonphotochemical processes; Area – the total area above the fluorescence induction curve representing the size of PQ pool on the reducing side of PSII; ETo/RC – electron transport flux per active reaction centre; ETo/CSo – phenomenological electron transport flux per leaf cross-section at the initial state; ETo/CSm – phenomenological electron transport flux per leaf cross-section at maximum fluorescence; RC/ABS – density of RCs per chlorophyll unit or absorption; RC/CSo – density of RCs per leaf cross-section at the initial state; RC/CSm – density of RCs per leaf cross-section at maximum fluorescence; PI_{abs} – performance index on an absorption basis integrating the density of reaction centres, the quantum yield of primary photochemistry, and the probability of electron transport; *df* – total driving force of photosynthesis based on fluorescence kinetics; PI_{tot} – total performance index, which incorporates the efficiency of the terminal electron acceptors of PSI.

photochemistry, with unequal seasonal trends and differing environmental responsiveness. A very high correlation was found only in closely related parameters (*e.g.*, ETo/CSo and ETo/CSm, F_v/F_m and F_v/F_o, *etc.*). PI_{abs} and *df* were fully correlated, as *df* represents the logarithm of PI_{abs}.

More important were the results of correlations with growth. Notably, the integrative indices PI_{tot}, PI_{abs}, and *df* showed exceptionally high positive correlations with the plant growth rate ($r = 0.98$ and $r = 0.79$, respectively). The leaf area was strongly correlated with ETo/RC ($r = 0.70$) and PI_{tot} ($r = 0.78$). As expected, F_v/F_m showed a more moderate, nonsignificant correlation with plant growth rate ($r = 0.51$), much lower than that for the integrative performance indices. Our findings indicate that PI_{tot}, PI_{abs}, and *df* are valid markers for monitoring the overall vitality of the photosynthetic apparatus, which is crucial for crop biomass accumulation during the wheat season.

To provide a more robust overall statistical analysis, we tested the effects of the two main factors present in the experiment (date and genotype) using two-way analysis of variance (Table 1). Our results clearly show the statistical significance of both factors and their interactions for all parameters assessed. While the study was not specifically focused on genotype assessment, it is worth noting that the method and parameters used demonstrated a good capacity to identify genotype-specific differences within a population of 30 varieties. Using effect size (partial eta squared), we found that genotype was a very strong factor for ETo/CSo and Area, but a less dominant factor for the performance indices. In turn, the date of measurement was a very strong factor for electron transport-related parameters and PI_{tot}, but less dominant for F_v/F_m and F_v/F_o. The interactions between the two factors were significant for all parameters.

In addition to this general statistical assessment, we also evaluated the stability of the measured fluorescence signals across the season by calculating the Theil Inequality Coefficient (U). We observed a clear hierarchy in signal stability: PI_{tot} (0.051) and F_v/F_m (0.060) exhibited the highest smoothness, while kinetic-derived parameters such as RC/ABS (0.138) displayed greater relative noise, which may be attributable to environmental fluctuations.

To evaluate the utility of different JIP-test parameters for crop phenotyping, we analysed the relationship between

Table 1. The values of statistical indicators related to analysis of variance (*ANOVA*) and assessment of trend-following accuracy in the plotted values. *** The effect of the factor is highly significant ($P<0.001$). $^{+++}$ U values are classified on a scale from perfect fit (0) to no fit (1). Area – the total area above the fluorescence induction curve representing the size of PQ pool on the reducing side of PSII; F_v/F_o – ratio of quantum yields of photochemical to nonphotochemical processes; F_v/F_m – maximum quantum yield of PSII; ETo/RC – electron transport flux per active reaction centre; RC/CSo – density of RCs per leaf cross-section at the initial state; ETo/CSo – phenomenological electron transport flux per leaf cross-section at the initial state; RC/CSm – density of RCs per leaf cross-section at maximum fluorescence; ETo/CSm – phenomenological electron transport flux per leaf cross-section at maximum fluorescence; RC/ABS – density of RCs per chlorophyll unit or absorption; PI_{abs} – performance index on an absorption basis integrating the density of reaction centres, the quantum yield of primary photochemistry, and the probability of electron transport; *df* – total driving force of photosynthesis based on fluorescence kinetics; PI_{tot} – total performance index, which incorporates the efficiency of the terminal electron acceptors of PSI.

Parameter	Effect size of factors (*ANOVA*) (partial eta squared)			Theil Inequality Coefficient (U)$^{+++}$
	Date	Genotype	Date × Genotype	Date
Area	0.21***	0.22***	0.43***	0.122
F_v/F_o	0.16***	0.13***	0.28***	0.111
F_v/F_m	0.15***	0.13***	0.24***	0.060
ETo/RC	0.60***	0.21***	0.37***	0.089
RC/CSo	0.55***	0.19***	0.53***	0.079
ETo/CSo	0.57***	0.23***	0.40***	0.081
RC/CSm	0.32***	0.17***	0.38***	0.093
ETo/CSm	0.44***	0.21***	0.31***	0.084
RC/ABS	0.16***	0.14***	0.37***	0.138
PI_{abs}	0.20***	0.12***	0.33***	0.075
df	0.19***	0.11***	0.33***	0.061
PI_{tot}	0.42***	0.10***	0.35***	0.051

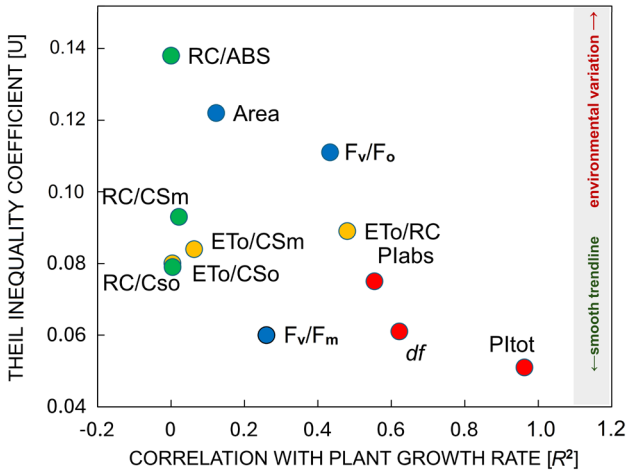

Fig. 8. Statistical framework for the sensitivity and predictability of photosynthetic parameters. Biplot relating the coefficient of determination (R^2) of the parameters correlated with plant growth rate to the Theil Inequality Coefficient assessing how closely the plotted values follow the predicted trend for each chlorophyll fluorescence parameter (excluding senescence period; shown by *dashed red lines* in Figs. 3–6). *The horizontal axis* represents the predictive power of a parameter for growth, while *the vertical axis* represents dataset noise attributed to fluctuating environmental factors during measurement.

their predictive power for growth and their unexplained variance (Fig. 8).

This statistical framework enabled us to categorise parameters by sensitivity. Parameters such as PI_{tot}, *df*, and PI_{abs}, clustered in the lower-right quadrant of the scatter plot, show high correlations with growth rate and lower noise (indicated by the Theil Inequality Coefficient, U). In particular, the PI_{tot} was identified as a parameter following the seasonal trend observed also in growth and productivity parameters, with relatively low noise in the data. Our observations suggest that this parameter can be exceptionally useful for monitoring the functional state and quantitative performance of the photosynthetic apparatus, with low noise caused by co-occurring environmental factors.

In contrast, parameters such as F_v/F_o, Area, and especially RC/ABS were positioned in the upper-left quadrant, exhibiting higher unexplained variance. These parameters were found to be more sensitive to transient environmental fluctuations and immediate physiological stress responses but do not have a good fit with a seasonal pattern of growth dynamics. This differentiation suggests that those parameters are useful for detecting effects of common environmental fluctuations. In the case of the F_v/F_m parameter, it showed quite smooth data, with relatively low noise, but its predictive capacity related to plant productivity in non-stressed plants used in our study was limited. A group of parameters clustered in the lower left indicate strong seasonality and low environmentally induced noise, but a low relationship with overall plant productivity.

Discussion

The implementation of a population-level phenomic approach, treating diverse wheat genotypes as a single population, significantly enhanced the robustness and

repeatability of the biophysical models established in this study. Our results (Fig. 2) demonstrate that by integrating a massive number of technical replicates across diverse genetic backgrounds, the resulting growth trajectories are smoothed, effectively minimising the stochastic measurement noise typical of low-throughput assays. As emphasised by Tsimilli-Michael (2020), plotting and examining raw transients within large replicate sets is essential to recognise data dispersion as critical information on natural biological heterogeneity rather than mere experimental error. This scale of analysis, supported by findings from Koller *et al*. (2020) and Begović *et al*. (2020), provides the statistical power necessary to detect subtle physiological shifts that would otherwise be masked. A key observation in our morphological data was that the peak in mean daily plant growth rate occurred between 210 and 230 d after sowing (DAS), several days after achieving maximum leaf area expansion at 215 DAS (Fig. 2). This lag suggests that maximum metabolic efficiency is reached not at the moment of maximum canopy size, but during a subsequent phase of physiological maturation where the newly expanded leaves reach their full carbon-assimilation potential. This longitudinal integration overcomes the inherent limitations of single-point measurements, which often capture only performance at a specific moment. Such snapshots are frequently biased by transient factors, including diurnal light fluctuations or temperature spikes (Živčák *et al*. 2014, Digrado *et al.* 2017).

The photosynthetic apparatus displays a clear hierarchy in parameter sensitivity throughout the season. For instance, the maximum quantum yield of primary photochemistry (F_v/F_m) remained remarkably high and stable (averaging 0.82–0.83) until 240 DAS, after which it dropped significantly (Fig. 3*A*). This stability, documented in various wheat cultivars (Lu *et al.* 2002, Yang *et al*. 2007), implies that the potential for primary PSII photochemistry is not the primary limiting bottleneck for biomass accumulation during the vegetative and early grain-filling phases. The maintenance of high F_v/F_m values suggests a surplus of PSII capacity, which is highly resistant to moderate environmental constraints (Cornic and Fresneau 2002, Desotgiu *et al.* 2012). However, our results demonstrate that F_v/F_o (Fig. 3*B*) is a far more sensitive precursor to physiological decline. Because F_v/F_o is mathematically magnified compared to the "ratio of extrema" seen in F_v/F_m, it captures subtle instabilities in the energetic balance within the photosynthetic units that F_v/F_m might mask (Banks 2017, Tsimilli-Michael 2020). Furthermore, the functional size of the plastoquinone pool, represented by the Area parameter (Fig. 3*C*), serves as a critical biophysical proxy for the total electron acceptor pool. The observed decline in Area during the post-anthesis period acts as a kinetic bottleneck; a smaller PQ pool provides fewer available slots for electron transfer, leading to an electron "traffic jam" that increases the probability of reaction centre closure (Holland *et al*. 2014, Stirbet *et al*. 2014).

Our analysis of reaction centre (RC) densities provides insight into the structural reorganisation of the light-harvesting apparatus during maturation. The divergence between densities expressed per unit area (RC/CSo) and per unit absorption (RC/ABS) (Fig. 5) reveals that maturation is not merely a quantitative increase in biomass, but a qualitative optimisation of energy distribution. Because RC/ABS is the reciprocal of the apparent antenna size, its movements relative to area-based metrics show how the plant balances its energy-harvesting "nets" against its "transformers" (Zeng *et al*. 2021). As leaves reach full expansion, the emergence of a gap between these parameters signals the transformation of some units into "silent reaction centres" that continue to absorb light but no longer contribute to the active pool (Strasser *et al*. 2004). While structural parameters like RC/ABS showed high temporal variability due to their role as dynamic sensors of environmental fluctuations, integrative indices remained stable. The precipitous drop in RC density during the final two samplings (Fig. 5*B*,*C*) signifies a programmed shift in metabolic hierarchy. As the flag leaf enters its final phase, it transitions from a "source" of carbohydrate to a critical reservoir for recycling nitrogen and minerals, with up to 75% of leaf nitrogen being reclaimed for the developing grains (Gregersen *et al*. 2008, Viljevac Vuletić *et al*. 2019). This dismantling represents a highly regulated adaptive program that prioritises nutrient remobilisation over the continued maintenance of the photosynthetic canopy (Zeng *et al*. 2021).

The superiority of integrative performance indices was a central finding of this study. The total performance index (PI_{tot}) exhibited significantly higher seasonal predictability (r^2 = 0.95, Fig. 6*C*) and a remarkably strong correlation with the mean daily plant growth rate (r = 0.98, Fig. 7) compared to the performance index on an absorption basis (PI_{abs}). This is primarily because PI_{tot} incorporates the δ_{Ro} component, describing the efficiency of electron transfer from the intersystem carriers to the terminal acceptors of PSI (Stirbet and Govindjee 2011). While PI_{abs} is restricted to events within PSII, PI_{tot} captures the cumulative energetic potential of the entire linear electron transport chain. In practical applications, PI_{tot} buffers the rapid, stochastic responses of PSII to environmental "noise" by accounting for the relatively more stable PSI capacity during maturation (Živčák *et al.* 2014). This makes PI_{tot} a far more responsive indicator of vitality, particularly under nutrient stress or during early-stage senescence, where it can detect functional declines as early as seven days after flowering (Špánić *et al*. 2023). Ultimately, because PI_{tot} accounts for the distal energetic bottlenecks that limit carbon fixation, it correlates more strongly with actual net CO_2 assimilation rates (Desotgiu *et al*. 2012).

The time series of parameters reveals varying degrees of temporal stability: some parameters exhibit clear, smooth trends, while others display considerable noise, with varying levels of deviation from their underlying trend. To quantify this variability, we applied Theil's Inequality Coefficient (U) as an analytical measure (Table 1). As referenced in the literature (Theil *et al.* 1961, Bellocchi *et al.* 2010), this coefficient provides a rigorous, multi-faceted validation of model performance that accounts for both systematic and unsystematic deviations from

the observed data. This allowed us to assess how closely the plotted (actual) values follow the predicted trend, on a scale from a perfect fit (0) to no predictive value (1). We observed a clear hierarchy in signal stability (Fig. 8) that serves as a robust quantitative proxy for a genotype's sensitivity to transient environmental fluctuations. Under stable conditions, biophysical parameters typically exhibit predictable relationships; however, the introduction of temperature spikes or moisture fluctuations increases "biophysical noise," causing a rise in unexplained variance (Stirbet *et al*. 2018, Begović *et al*. 2020). Our analysis demonstrates that while traditional parameters like F_v/F_m exhibit higher levels of noise, integrative indices like PI_{tot} better follow the underlying ontogenetic signal with lower effects of environmental fluctuations.

While the aggregation of diverse genotypes into a single population serves to reveal universal seasonal patterns, we recognise the importance of genotypic variability for breeding applications. We justify this population-level approach as a prerequisite for establishing a stable biophysical baseline, effectively suppressing the "genetic noise" that often masks fundamental photosynthetic dynamics. To address the fundamental importance of G × E interactions, we supplemented our population-level models with a multifactorial *ANOVA* (Table 1), which quantifies the variance attributed to the factor "GENOTYPE". This hierarchical statistical framework allows us to define the species-level ontogenetic progression while concurrently providing the variance-partitioning tools necessary to identify high-performing genotypes that deviate from this established population baseline. Therefore, although genotype comparison, frequently applied in previous investigations (Živčák *et al*. 2008, Begović *et al*. 2020, Spanic *et al*. 2021), was not among the aims of this study, our statistical analysis shows that the method and individual parameters can detect genotypic variation across the season, in addition to seasonal trends. This indicates that our results have applicability beyond a purely developmental perspective.

Translating this biophysical framework into a practical breeding protocol requires prioritising integrative indices, such as PI_{tot} and PI_{abs}, over primary yield measurements. Performance indices are calculated by combining parameters related to the density of active PSII reaction centres, the quantum yield of photochemistry, and the efficiency of electron transport steps. Together, these indices provide a comprehensive evaluation of the photosynthetic apparatus's vitality by quantifying the plant's ability to conserve energy and effectively drive linear electron transport (Stirbet *et al.* 2018). Performance indices derived from the JIP-test are considered more informative than single OJIP-derived parameters, as they integrate multiple partial reactions of the photosynthetic electron transport chain (Strasser *et al*. 2000, 2004). Because PIs incorporate several structural and functional parameters, including the density of active reaction centres, the efficiency of exciton trapping, and electron transport beyond Q_A^-, they provide a more comprehensive and sensitive readout of stress-induced perturbations across the whole photosynthetic apparatus. Moreover, since PIs are calculated as products of multiple normalised sub-components, even small stress-induced changes in individual parameters can be amplified in the composite index, further enhancing overall sensitivity (Stirbet *et al*. 2018). Small shifts in the redox state of individual electron transport chain components – arising from variation in actual environmental conditions that directly influence chloroplast processes can be effectively compensated for, since an increase in one component's redox state can be offset by a decrease in a subsequent component. As a result, performance indices (PIs), especially PI_{tot}, that integrate multiple functional traits may show lower overall variability and noise than parameters describing a single functional trait (Živčák *et al*. 2014).

In addition to multiple stress-related applications (Kalaji *et al*. 2016), these indices, for example, facilitate the selection of "functional stay-green" varieties that balance nutrient remobilisation with sustained photosynthetic activity. This is particularly valuable given the positive correlation between flag leaf longevity and total yield (Carmo-Silva *et al*. 2017, Galić *et al*. 2020, Spanic *et al*. 2021). Nevertheless, to integrate these robust multivariate physiological readouts into a unified statistical framework, it is necessary to move beyond simple snapshot evaluations toward a dynamic, holistic understanding of plant performance throughout the growing season, as was done in our study.

On the other hand, we recognise that our study has several limitations. First, the single-site, single-season nature of this study limits the geographic generalisability of our findings. However, we assert that the high-resolution longitudinal temporal density achieved here (nine sampling events across the life cycle) provides a unique "biophysical chronosequence" useful for defining the fundamental ontogenetic signature of wheat. While multi-site validation is required to assess environmental robustness across diverse pedoclimatic zones, this study establishes the critical species-level baseline necessary to calibrate such future efforts.

The second limitation is the lack of direct measurements of photosynthetic parameters, such as gas-exchange data. However, it is well established that systems available for directly measuring photosynthetic capacity have low throughput, which creates a bottleneck for larger-scale research activities (Salter *et al*. 2018). This makes such measurements unrealistic to perform at the required extent and quality, given the time needed per measurement and the relatively narrow daily window during which correct measurements can be taken (Haworth *et al*. 2018). In addition, our study does not rely solely on the theoretical link between fluorescence and photochemistry; it is anchored by a high-resolution, longitudinal, and labour-intensive assessment of plant growth, leaf area, and biomass accumulation. This provides an extremely valuable dataset representing the net result of carbon assimilation – namely, cumulative dry mass and its rate of change. These results can therefore serve as an adequate real-world benchmark against which the fluorescence indices were tested. Nevertheless, we believe that analysing leaf-scale photosynthetic

performance and limitations alongside fluorescence and growth data would add an important additional layer of information, and we regard this as a valuable direction for future research.

Acknowledging these limitations, we propose that our findings serve primarily as a valuable proof-of-concept, providing a standardised temporal framework against which future multi-year, multi-environment data can be systematically compared.

Conclusions: The presented results demonstrate that the complex physiological fingerprint provided by fast chlorophyll fluorescence can be systematically deconstructed to distinguish between long-term ontogenetic programming and transient environmental responses in winter wheat. By employing a longitudinal phenomic approach across a diverse multi-genotype population, we have successfully established a hierarchical framework for the interpretation of JIP-test parameters. Our findings reveal that integrative performance indices, most notably the total performance index (PI_{tot}), may serve as robust indicators of photosynthetic vitality, associated with seasonal growth dynamics and biomass accumulation. A high correlation between PI_{tot} and plant growth rate, coupled with its low unexplained variance, positions this parameter as a valid marker for assessing the holistic vitality of the photosynthetic apparatus. Unlike basic fluorescence ratios, PI_{tot} effectively integrates the efficiencies of both Photosystem II and Photosystem I, thereby providing a more faithful representation of the plant's actual carbon-assimilation potential throughout the vegetative and reproductive phases.

In contrast, our analysis highlights a clear functional divergence for traditional parameters such as the maximum quantum yield of primary photochemistry ratio (F_v/F_m). While these parameters are sensitive detectors of acute environmental stressors and terminal leaf senescence, they exhibit significantly higher levels of unexplained variance in relation to seasonal growth trajectories. Consequently, while they remain invaluable for identifying significant photochemical damage or transient acclimatory shifts, they do not provide a reliable metric for quantitative photosynthetic performance or yield-related phenotyping. This differentiation is critical for the advancement of high-throughput phenotyping; it suggests that breeding programs should prioritise integrative indices to monitor cumulative vigour, while reserving primary quantum yields for the detection of specific stress-induced injuries.

Ultimately, the statistical framework developed in this study provides useful insights into the phenomic gap in field-based research. By identifying which biophysical markers are predominantly ontogenetic signatures *vs.* those that are environmentally responsive, we enable a more precise physiological interpretation of large-scale fluorescence datasets. This approach facilitates the development of more stable and repeatable phenotypic models, which are essential for the selection of superior genotypes with improved photosynthetic efficiency and climate resilience. The ability to noninvasively monitor the linear electron transport chain's stepwise reduction with such high seasonal predictability marks a valid step toward integrating mechanistic biophysical knowledge into the broader context of crop improvement and precision agriculture.

References

Banks J.M.: Continuous excitation chlorophyll fluorescence parameters: a review for practitioners. – Tree Physiol. **37**: 1128-1136, 2017.

Begović L., Galić V., Abicić I. *et al.*: Implications of intra-seasonal climate variations on chlorophyll *a* fluorescence and biomass in winter barley breeding program. – Photosynthetica **58**: 995-1008, 2020.

Bellocchi G., Rivington M., Donatelli M., Matthews K.: Validation of biophysical models: issues and methodologies. A review. – Agron. Sustain. Dev. **30**: 109-130, 2010.

Butler W.L., Kitajima M.: Fluorescence quenching in photosystem II of chloroplasts. – BBA-Bioenergetics **376**: 116-125, 1975.

Carmo-Silva E., Andralojc P.J., Scales J.C. *et al.*: Phenotyping of field-grown wheat in the UK highlights contribution of light response of photosynthesis and flag leaf longevity to grain yield. – J. Exp. Bot. **68**: 3473-3486, 2017.

Ceppi M.G., Oukarroum A., Çiçek N. *et al.*: The IP amplitude of the fluorescence rise OJIP is sensitive to changes in the photosystem I content of leaves: a study on plants exposed to magnesium and sulfate deficiencies, drought stress and salt stress. – Physiol. Plantarum **144**: 277-288, 2012.

Cornic G., Fresneau C.: Photosynthetic carbon reduction and carbon oxidation cycles are the main electron sinks for photosystem II activity during a mild drought. – Ann. Bot.-London **89**: 887-894, 2002.

Desotgiu R., Cascio C., Pollastrini M. *et al.*: Short and long term photosynthetic adjustments in sun and shade leaves of *Fagus sylvatica* L., investigated by fluorescence transient (FT) analysis. – Plant Biosyst. **146**: 206-216, 2012.

Digrado A., Bachy A., Mozaffar A. *et al.*: Long-term measurements of chlorophyll *a* fluorescence using the JIP-test show that combined abiotic stresses influence the photosynthetic performance of the perennial ryegrass (*Lolium perenne*) in a managed temperate grassland. – Physiol. Plantarum **161**: 355-371, 2017.

Galić V., Mazur M., Šimić D. *et al.*: Plant biomass in salt-stressed young maise plants can be modelled with photosynthetic performance. – Photosynthetica **58**: 194-204, 2020.

Gaudio N., Escobar-Gutiérrez A.J., Casadebaig P. *et al.*: Current knowledge and future research opportunities for modeling annual crop mixtures. A review. – Agron. Sustain. Dev. **39**: 20, 2019.

Gregersen P.L., Holm P.B., Krupinska K.: Leaf senescence and nutrient remobilisation in barley and wheat. – Plant Biol. **10**: 37-49, 2008.

Haworth M., Marino G., Centritto M.: An introductory guide to gas exchange analysis of photosynthesis and its application to plant phenotyping and precision irrigation to enhance water use efficiency. – J. Water Clim. Change **9**: 786-808, 2018.

Holland V., Koller S., Brüggemann W.: Insight into the photosynthetic apparatus in evergreen and deciduous European oaks during autumn senescence using OJIP fluorescence transient analysis. – Plant Biol. **16**: 801-808, 2014.

Kalaji H.M., Jajoo A., Oukarroum A. *et al.*: Chlorophyll *a* fluorescence as a tool to monitor physiological status of plants under abiotic stress conditions. – Acta Physiol. Plant. **38**: 102, 2016.

Kalaji H.M., Schansker G., Ladle R.J. *et al.*: Frequently asked questions about chlorophyll fluorescence: practical issues. – Photosynth. Res. **122**: 121-158, 2014.

Koller S., Holland V., Brüggemann W.: Seasonal monitoring of PSII functionality and relative chlorophyll content on a field site in two consecutive years: a case study of different oak species. – Photosynthetica **58**: 379-390, 2020.

Lu Q., Lu C., Zhang J., Kuang T.: Photosynthesis and chlorophyll *a* fluorescence during flag leaf senescence of field-grown wheat plants. – J. Plant Physiol. **159**: 1173-1178, 2002.

Miralles D.J., Slafer G.A.: A simple model for nondestructive estimates of leaf area in wheat. – Cereal Res. Commun. **19**: 439-444, 1991.

Pandey A.K., Jiang L., Moshelion M. *et al.*: Functional physiological phenotyping with functional mapping: A general framework to bridge the phenotype-genotype gap in plant physiology. – iScience **24**: 102846, 2021.

Prakash J.S.S., Srivastava A., Strasser R.J., Mohanty P.: Senescence induced alterations in the photosystem II functions of *Cucumis sativus* cotyledons: probing of senescence driven alterations of photosystem II by chlorophyll *a* fluorescence induction O-J-I-P transients. – Indian J. Biochem. Bio. **40**: 160-168, 2003.

Salter W.T., Gilbert M.E., Buckley T.N.: A multiplexed gas exchange system for increased throughput of photosynthetic capacity measurements. – Plant Methods **14**: 80, 2018.

Schansker G., Tóth S.Z., Strasser R.J.: Methylviologen and dibromothymoquinone treatments of pea leaves reveal the role of photosystem I in the Chl *a* fluorescence rise OJIP. – BBA-Bioenergetics **1706**: 250-261, 2005.

Siebers M.H., Gomez-Casanovas N., Fu P. *et al.*: Emerging approaches to measure photosynthesis from the leaf to the ecosystem. – Emerg. Top. Life Sci. **5**: 261-274, 2021.

Spanic V., Mlinaric S., Zdunic Z., Katanic Z.: Field study of the effects of two different environmental conditions on wheat productivity and chlorophyll fluorescence induction (OJIP) parameters. – Agriculture **11**: 1154, 2021.

Stirbet A., Govindjee: On the relation between the Kautsky effect (chlorophyll *a* fluorescence induction) and photosystem II: Basics and applications of the OJIP fluorescence transient. – J. Photoch. Photobio. B **104**: 236-257, 2011.

Stirbet A., Lazár D., Kromdijk J., Govindjee: Chlorophyll *a* fluorescence induction: Can just a one-second measurement be used to quantify abiotic stress responses? – Photosynthetica **56**: 86-104, 2018.

Stirbet A., Riznichenko G.Yu., Rubin A.B., Govindjee: Modeling chlorophyll *a* fluorescence transient: relation to photosynthesis. – Biochemistry-Moscow **79**: 291-323, 2014.

Strasser B.J., Strasser R.J.: Measuring fast fluorescence transients to address environmental questions: the JIP test. – In: Mathis P. (Ed.): Photosynthesis: From Light to Biosphere. Vol. 5. Pp. 977-980. Kluwer Academic Publishers, Dordrecht 1995.

Strasser R.J., Srivastava A., Govindjee: Polyphasic chlorophyll *a* fluorescence transient in plants and cyanobacteria. – Photochem. Photobiol. **61**: 32-42, 1995.

Strasser R.J., Srivastava A., Tsimilli-Michael M.: The fluorescence transient as a tool to characterize and screen photosynthetic samples. – In: Yunus M., Pathre U., Mohanty P. (Eds.): Probing Photosynthesis: Mechanisms, Regulation and Adaptation. Pp. 445-483. Taylor & Francis, London 2000.

Strasser R.J., Tsimilli-Michael M., Srivastava A.: Analysis of the chlorophyll *a* fluorescence transient. – In: Papageorgiou G.C., Govindjee (Eds.): Chlorophyll *a* Fluorescence: A Signature of Photosynthesis. Advances in Photosynthesis and Respiration. Pp. 321-362. Springer, Dordrecht 2004.

Španić V., Šunić K., Duvnjak J. *et al.*: Chlorophyll *a* fluorescence during flag leaf senescence of field-grown winter wheat plants under drought conditions. – Ann. Appl. Biol. **183**: 80-92, 2023.

Theil H., Cramer J.S., Moerman H., Russchen A.: Economic Forecast and Policy. 2nd Edition. Pp. 567. North-Holland Publishing Company, Amsterdam 1961.

Thomas H., Ougham H.: The stay-green trait. – J. Exp. Bot. **65**: 3889-3900, 2014.

Tsimilli-Michael M., Strasser R.J.: *In vivo* assessment of stress impact on plants' vitality: applications in detecting and evaluating the beneficial role of mycorrhization on host plants. – In: Varma A. (Ed.): Mycorrhiza. State of the Art, Genetics and Molecular Biology, Eco-Function, Biotechnology, Eco-Physiology, Structure and Systematics. 3rd Edition. Pp. 679-703. Springer, Berlin-Heidelberg 2008.

Tsimilli-Michael M.: Revisiting JIP-test: An educative review on concepts, assumptions, approximations, definitions and terminology. – Photosynthetica **58**: 275-292, 2020.

Viljevac Vuletić M., Marček T., Španić V.: Photosynthetic and antioxidative strategies of flag leaf maturation and its impact to grain yield of two field-grown wheat varieties. – Theor. Exp. Plant Phys. **31**: 387-399, 2019.

Viljevac Vuletić M., Španić V.: Characterization of photosynthetic performance during natural leaf senescence in winter wheat: multivariate analysis as a tool for phenotypic characterization. – Photosynthetica **58**: 301-313, 2020.

Yang D.-L., Jing R.-L., Chang X.-P., Li W.: Quantitative trait loci mapping for chlorophyll fluorescence and associated traits in wheat (*Triticum aestivum*). – J. Integr. Plant Biol. **49**: 646-654, 2007.

Yoo C., Gonzalez E., Gong Z., Roy D.: A better mechanistic understanding of big data through an order search using causal Bayesian networks. – Big Data Cogn. Comput. **6**: 56, 2022.

Zeng F., Wang G., Liang Y. *et al.*: Disentangling the photosynthesis performance in japonica rice during natural leaf senescence using OJIP fluorescence transient analysis. – Funct. Plant Biol. **48**: 206-217, 2021.

Zhang P., Huang J., Ma Y. *et al.*: Crop/plant modeling supports plant breeding: II. Guidance of functional plant phenotyping for trait discovery. – Plant Phenomics **5**: 0091, 2023.

Živčák M., Brestič M., Olšovská K., Slamka P.: Performance index as a sensitive indicator of water stress in *Triticum aestivum* L. – Plant Soil Environ. **54**: 133-139, 2008.

Živčák M., Olšovská K., Slamka P. *et al.*: Application of chlorophyll fluorescence performance indices to assess the wheat photosynthetic functions influenced by nitrogen deficiency. – Plant Soil Environ. **60**: 210-215, 2014.